Inorg. Chem. **2009**, *48*, 508−517

Effects of ZSM-5 Zeolite Confinement on Reaction Intermediates during Dioxygen Activation by Enclosed Dicopper Cations

Takashi Yumura,*,† Mina Takeuchi,† Hisayoshi Kobayashi,† and Yasushige Kuroda‡

Department of Chemistry and Materials Technology, Kyoto Institute of Technology, Matsugasaki, Sakyo-ku, Kyoto, 606-8585, Japan, and Department of Fundamental Material Science, Division of Molecular and Material Science, Graduate School of Natural Science and Technology, Okayama University, Tsushima, Okayama 700-8530, Japan

Received June 3, 2008

We investigate how nanospaces surrounded by a 10-membered ring of ZSM-5 zeolite affect the reaction intermediates formed during dioxygen activation by enclosed dicopper cations. Two types of dioxygen intermediates are considered: one is an $O_2\cdots Cu_2$ complex, where dioxygen binds to the two Cu cations, and the other is a bis(μ-oxo)dicopper complex converted from an $O_2\cdots Cu_2$ complex by the cleavage of the O−O bond. We employ large-scale density functional theory (DFT) calculations with the B3LYP functional to examine the energetics of the two dioxygen intermediates inside a 10-membered ring of ZSM-5 with double Si → Al substitutions at variable locations. The properties of the $O_2\cdots Cu_2$ complexes, such as the dioxygen bridging modes and dioxygen activation, are strongly affected by the locations of the two Al atoms within the 10-membered ring. In particular, the $O_2\cdots Cu_2$ complexes have either end-on or side-on bridging modes depending on the substituted Al positions. On the other hand, the steric hindrances of a ZSM-5 cavity play crucial roles in determining the properties of the bis(μ-oxo)dicopper complexes containing a diamond Cu_2O_2 core. By restricting its Cu_2O_2 core to a 10-membered ring of ZSM-5 in which the two Al atoms are second-nearest neighbors, each Cu cation is tetrahedral four-coordinate. On the other hand, the Cu cations have almost square planar coordination inside a ZSM-5 where the Al atoms are fourth-nearest neighbors. The different Cu coordination environments are responsible for the different levels of stability; the planar diamond Cu_2O_2 core is 30.7 kcal/mol more stable relative to the tetrahedral case. Since the ZSM-5 nanospaces directly influence the stability of the bis(μ-oxo)dicopper complexes by changing the Cu coordination environments, zeolite confinement effects on the bis(μ-oxo)dicopper complexes are more noticeable than those in the $O_2\cdots Cu_2$ cases. The DFT findings are important in terms of catalytic functions, because the spatial constraint from the ZSM-5 should significantly contribute to the stability of the reaction intermediates formed during the dioxygen activation.

Introduction

Zeolites, which are aluminosilicate-based materials, have inner cavities with diameters at the nanometer scale.[1] By encapsulating various molecules into their cavities, they can become novel host−guest materials.[2] In fact, zeolites can act as molecular sieves, and consequently the restricted environment of a zeolite host should have an influence on the chemical reactions that take place within the zeolite. Another characteristic is that substituting Al^{3+} for Si^{4+} in SiO_2 frameworks introduces negative charges on the oxygen atoms in the neighboring sites. Because of the charge balance requirement, a wide range of cations (e.g., Na^+ and K^+) can be accommodated in an inner cavity and be loosely bound to its framework. The loosely bound cations can be exchanged for transition-metal cations.[3] The trapping of transition-metal cations gives zeolites additional catalytic functions due to the high chemical reactivities of transition-metal cations. Accordingly, zeolites have been utilized as nanoporous catalysts in a wide range of industrial applications.[4,5]

* To whom correspondence should be addressed. E-mail: yumura@chem.kit.ac.jp.
† Kyoto Institute of Technology.
‡ Okayama University.

(1) Baelocher, Ch.; Meier, W. M.; Olson, D. H. *Atlas of Zeolite Framework Types*, 5th ed.; Elsevier: Amsterdam, 2001.
(2) Huheey, J. E. *Inorganic Chemistry*, 4th ed.; Harper & Row: New York, 1993.
(3) Shelef, M. *Chem. Rev.* **1995**, *95*, 209.
(4) Corma, A. *Chem. Rev.* **1995**, *95*, 559.

10.1021/ic8010184 CCC: $40.75
Published on Web 12/18/2008

One of the most successful ion-exchanged zeolites is copper-exchanged ZSM-5 (Cu−ZSM-5),[6−14] because it catalyzes NO decomposition and reduction. The ZSM-5 structure consists of 5- and 6-membered rings (MRs) on channel walls, and 10-MRs in straight and sinusoidal channels. Schoonheydt and co-workers recently reported that, in addition to its catalytic activity, Cu−ZSM-5 can also convert methane and dioxygen into methanol.[15] The direct methane oxidation is reminiscent of the oxidation ability of membrane-bound particulates of methane monooxygenase (pMMO) containing mononuclear and dinuclear copper species as active sites.[16−19] Since Cu−ZSM-5 seems to mimic the catalytic functions of the enzyme, many researchers have attempted to identify a reaction mechanism for the direct methane oxidation by Cu−ZSM-5.

A possible mechanism has been proposed[15] by analogy with the biological system, together with its relevant synthetic models,[20,21] as given in Scheme 1. In the first step, dioxygen binds to two Cu(I) centers[14e] in a side-on fashion to generate an $O_2\cdots Cu_2$ complex where each Cu cation has a formal charge of +2. After that, the dioxygen O−O bond in the resultant $O_2\cdots Cu_2$ complex is activated, leading to a bis(μ-oxo)dicopper(III) complex, which is responsible for the direct methane oxidation. The proposed reaction mechanism is based on experimental results that have indicated the presence of Cu pairs in ZSM-5.[6−14] In particular, extended X-ray absorption fine structure (EXAFS) spectroscopy studies have revealed that the separations of Cu pairs fall in the range of 2.47−3.13 Å.[11−14] In line with the experimental proposals, Goodman and co-workers used density functional theory (DFT) calculations to investigate the properties of the dioxygen intermediates in ZSM-5 modeled by $Al_2(OH)_8$ or slightly larger clusters ($Al_2Si_7O_{26}H_{16}$ and $Al_2Si_8O_{29}H_{18}$).[22] According to their pioneering work,[22] the bis(μ-oxo)dicopper complex, as well as the side-on peroxo complex, are energetically preferable when the separations between the two Cu cations range from 2.5 to 3.7 Å.

Scheme 1

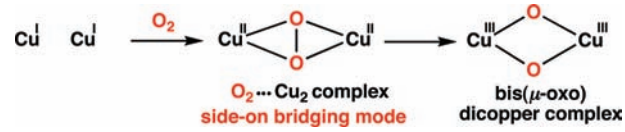

A fundamental question arises as to where Cu cations sit within the real ZSM-5 framework. To answer this question, Mentzen and co-workers recently used the Rietveld method of X-ray powder diffraction (XRPD) to examine the locations of Cu cations within the ZSM-5 framework with a certain Si/Al substitution ratio.[23] Their analysis revealed that the Cu cations are located near the wall of 10-MRs of straight channels, and the narrowest Cu··Cu separation is 4.33 Å, substantially longer than those obtained in the EXAFS analyses.[11−14] The Cu cations within 10-MRs should be responsible for the catalytic activity, due to the facile entry of guest molecules such as dioxygen and methane into the cations. Despite the importance of the Cu cations located in the vicinity of their 10-MRs, the effects of zeolite nanospaces on the reaction intermediates formed during the dioxygen activation have remained relatively unexplored. In the present study, we use large-scale DFT calculations to investigate how the restricted environment of a 10-MR in ZSM-5 affects the dioxygen intermediates ($O_2\cdots Cu_2$ complexes and bis(μ-oxo)dicopper complexes).

Method of Calculation

To date, zeolite systems have been theoretically investigated using both cluster-model[24−37] and periodic boundary condition (PBC) calculations.[38,39] For PBC calculations of ZSM-5, a large unit cell (20.1 Å × 19.7 Å × 13.1 Å) including 288 atoms is required. Due to the limitations of our computational resources,

(5) van Santen, R. A.; Kramer, G. J. *Chem. Rev.* **1995**, *95*, 637.
(6) (a) Iwamoto, M.; Furukawa, H.; Mine, Y.; Uemura, F.; Mikuriya, S.; Kagawa, S. *J. Chem. Soc., Chem. Commun.* **1986**, 1272. (b) Iwamoto, M.; Yahiro, H.; Tanda, K.; Mizuno, N.; Mine, Y.; Kagawa, S. *J. Phys. Chem.* **1991**, *95*, 3727. (c) Iwamoto, M.; Yahiro, H.; Mizuno, N.; Zhang, W.-X.; Mine, Y.; Furukawa, H.; Kagawa, S. *J. Phys. Chem. B* **1991**, *96*, 9360.
(7) (a) Li, Y.; Keith Hall, W. *J. Catal.* **1991**, *129*, 202. (b) Keith Hall, W.; Vaylon, J. *Catal. Lett.* **1992**, *15*, 311. (c) Jong, H. J.; Keith Hall, W.; d'Itri, J. L. *J. Phys. Chem.* **1996**, *100*, 9416.
(8) Sárkány, J.; d'Itri, J. L.; Sachtler, M. H. *Catal. Lett.* **1992**, *16*, 241.
(9) Costa, P. S.; Modén, B.; Meitzner, G. D.; Lee, D. K.; Iglesia, E. *Phys. Chem. Chem. Phys.* **2002**, *4*, 4590.
(10) Anpo, M.; Matsuoka, M.; Shioya, Y.; Yamashita, H.; Giamello, E.; Morterra, C.; Che, M.; Patterson, H. H.; Webber, S.; Ouellette, S.; Fox, M. A. *J. Phys. Chem.* **1994**, *98*, 5744.
(11) Palomino, G. T.; Fisicaro, P.; Bordiga, S.; Zecchina, A.; Giamello, E.; Lamberti, C. *J. Phys. Chem. B* **2000**, *104*, 4064.
(12) Hamada, H.; Matsubayashi, N.; Shimada, H.; Kintaichi, Y.; Ito, T.; Nishijima, A. *Catal. Lett.* **1990**, *5*, 189.
(13) Grünert, W.; Hayes, N. W.; Joyner, R. W.; Shpiro, E. S.; Siddiqui, M. R. H.; Baeva, G. N. *J. Phys. Chem.* **1994**, *98*, 10832.
(14) (a) Kumashiro, R.; Kuroda, Y.; Nagao, M. *J. Phys. Chem. B* **1999**, *103*, 89. (b) Kuroda, Y.; Kumashiro, R.; Yoshimoto, T.; Nagao, M. *Phys. Chem. Chem. Phys.* **1999**, *1*, 649. (c) Kuroda, Y.; Yagi, K.; Horiguchi, N.; Yoshikawa, Y.; Kumashiro, R.; Nagao, M. *Phys. Chem. Chem. Phys.* **2003**, *5*, 3318. (d) Itadani, A.; Tanaka, M.; Mori, T.; Nagao, M.; Kobayashi, H.; Kuroda, Y. *J. Phys. Chem. C* **2007**, *111*, 12011. (e) Itadani, A.; Tanaka, M.; Kuroda, Y.; Nagao, M. *New J. Chem.* **2007**, *31*, 1681.
(15) (a) Groothaert, M. H.; van Bokhoven, J. A.; Battiston, A. A.; Weckhuysen, B. M.; Schoonheydt, R. A. *J. Am. Chem. Soc.* **2003**, *125*, 7629. (b) Groothaert, M. H.; Smeets, P. J.; Sels, B. F.; Jacob, P. A.; Schoonheydt, R. A. *J. Am. Chem. Soc.* **2005**, *127*, 1394.
(16) Lieberman, R. L.; Rosenzweig, A. C. *Nature* **2005**, *434*, 177.
(17) Chan, S. I.; Chen, K. H.-C.; Yu, S. S.-F.; Chen, C.-L.; Kuo, S. S.-J. *Biochemistry* **2004**, *43*, 4421.
(18) Lieberman, R. L.; Shrestha, D. B.; Doan, P. E.; Hoffman, B. M.; Stemmler, T. L.; Rosenzweig, A. C. *Proc. Natl. Acad. Sci. U.S.A.* **2003**, *100*, 3820.
(19) (a) Yoshizawa, K.; Shiota, Y. *J. Am. Chem. Soc.* **2006**, *128*, 9873. (b) Yoshizawa, K. *Acc. Chem. Res.* **2006**, *39*, 375.
(20) Kitajima, N.; Fujisawa, K.; Fujimoto, C.; Moro-oka, Y.; Hashimoto, S.; Kitagawa, T.; Toriumi, K.; Tatsumi, K.; Nakamura, A. *J. Am. Chem. Soc.* **1992**, *114*, 1277.
(21) See important reviews: (a) Que, L.; Tolman, W. B. *Angew. Chem., Int. Ed.* **2002**, *41*, 1114. (b) Solomon, E. I.; Sarangi, R.; Woertink, J. S.; Augustine, A. J.; Yoon, J.; Ghosh, S. *Acc. Chem. Res.* **2007**, *40*, 581. (c) Itoh, S.; Fukuzumi, S. *Acc. Chem. Res.* **2007**, *40*, 592.
(22) (a) Goodman, B. R.; Schneider, W. F.; Hass, K. C.; Adams, J. B. *Catal. Lett.* **1999**, *1*, 639. (b) Goodman, B. R.; Hass, K. C.; Schneider, W. F.; Adams, J. B. *J. Phys. Chem. B* **1999**, *103*, 10452.
(23) (a) Mentzen, B. F.; Bergeret, G.; Emerich, H.; Weber, H.-P. *J. Phys. Chem. B* **2006**, *110*, 97. (b) Mentzen, B. F.; Bergeret, G. *J. Phys. Chem. C* **2007**, *111*, 12512.
(24) Corma, A.; García, H.; Sastre, G.; Viruela, P. M. *J. Phys. Chem. B* **1997**, *101*, 4575.
(25) Gonzales, N. O.; Bell, A. T.; Chakraborty, A. K. *J. Phys. Chem. B* **1997**, *101*, 10058.
(26) Hass, K. C.; Schneider, W. F. *Phys. Chem. Chem. Phys.* **1999**, *1*, 639.
(27) Zygmunt, S. A.; Curtiss, L. A.; Zapol, P.; Iton, L. E. *J. Phys. Chem. B* **2000**, *104*, 1944.

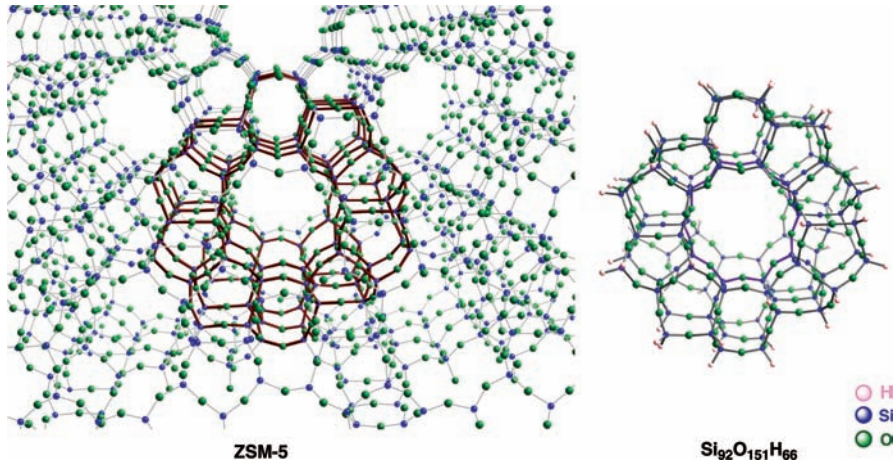

Figure 1. Structures of ZSM-5 zeolite and a model aluminum-free ZSM-5 zeolite, $Si_{92}O_{151}H_{66}$. The model corresponds to the red part in ZSM-5, and the terminal atoms are saturated by H atoms.

PBC calculations with sufficiently flexible plane-wave basis sets are not feasible at the present time. As an alternative, cluster-model calculations have employed quantum mechanics (QM) methods[23−31] and hybrid quantum mechanics/molecular mechanics (QM/MM) methods.[32−37] In the QM/MM methods, a cluster model is divided into two regions: an inner region in the vicinity of an active site, which is treated with a high-accuracy QM method, and an outer environment, which is treated with a low-accuracy MM method. In previous QM studies, the number of atoms in the cluster models was limited for computational efficiency, and thus these studies sometimes failed to elucidate the unique properties of an active site inside a zeolite. In contrast, hybrid QM/MM methods can be promising tools to investigate catalytic functions of an active site, because the zeolite surroundings can be treated with a low-accuracy method. In the hybrid methods, the size of the inner region around an active site plays a crucial role in accurately estimating the various reaction profiles, particularly the geometries of the active site, the heats of reaction, and the barrier heights.[34] One of the authors investigated covalent bond formation in a different type of host−guest material, a nanopeapod where fullerene molecules are encapsulated inside a carbon nanotube, and found that the covalent bonds formed between a nanotube host and a deformed fullerene guest modify the host surface in a large region.[40] This indicates that the structure of the ZSM-5 host may be significantly deformed by the interactions with a Cu_2O_2 guest. However, our knowledge about how the coordination of a Cu_2O_2 guest to the ZSM-5 host perturbs the host structure is incomplete. As a result, we do not have definitive information on the most suitable size for the inner region of Cu−ZSM-5 in order to describe its catalytic function properly using the hybrid methods.

Given the disadvantages in the previous theoretical studies, we carried out a QM calculation with a ZSM-5 cluster large enough to clarify the roles of nanospaces surrounded by 10-MRs in the catalytic functions of Cu−ZSM-5. In the present study, we used the B3LYP method as a QM method implemented in the Gaussian 03 software package.[41] The B3LYP functional[42,43] consists of the Slater exchange, the Hartree−Fock exchange, the exchange functional of Becke,[42a] the correlation functional of Lee, Yang, and Parr (LYP),[43] and the correlation functional of Vosko, Wilk, and Nusair (VWN).[44] As a model of aluminum-free ZSM-5,[45] we adopt a $Si_{92}O_{151}H_{66}$ cluster where the terminal atoms are bound to H atoms, as shown in Figure 1. The model corresponds to the red part of the ZSM-5 framework (Figure 1, left)[45] and explicitly contains 10-MRs of ZSM-5. To check whether the model is suitable to represent a 10-MR cavity of ZSM-5, we fully optimized the $Si_{92}O_{151}H_{66}$ structure at the B3LYP/3-21G level of the theory.[46] In the optimized geometry of Figure 1, right, the separations between two diametrically opposed Si atoms within the purple 10-MR are only 3% longer than those obtained experimentally.[45] Therefore, the chosen model is appropriate for the present study.

(28) (a) Yoshizawa, K.; Yumura, T.; Shiota, Y.; Yamabe, T. *Bull. Chem. Soc. Jpn.* **2000**, *73*, 29. (b) Yoshizawa, K.; Shiota, Y.; Yumura, T.; Yamabe, T. *J. Phys. Chem. B* **2000**, *104*, 734. (c) Yoshizawa, K.; Shiota, Y.; Kamachi, T. *J. Phys. Chem. B* **2003**, *107*, 11404.

(29) Shubin, A. A.; Zhidomirov, G. M.; Yakovlev, A. L.; van Santen, R. A. *J. Phys. Chem. B* **2001**, *105*, 4928.

(30) Morpurgo, S.; Moretti, G.; Bossa, M. *Phys. Chem. Chem. Phys.* **2007**, *9*, 417.

(31) Zheng, X.; Zhang, Y.; Bell, A. T. *J. Phys. Chem. C* **2007**, *111*, 13442.

(32) Pantu, P.; Pabchanda, S.; Limtrakul, J. *ChemPhysChem* **2004**, *5*, 1901.

(33) Shor, E. A. I.; Shor, A. M.; Nasluzov, V. A.; Vayssilov, G. N.; Rösch, N. *J. Chem. Theory Comput.* **2005**, *1*, 459.

(34) Fermann, J. T.; Moniz, T.; Kiowski, O.; McIntire, T. J.; Auerbach, S. M.; Vreven, T.; Frisch, M. J. *J. Chem. Theory Comput.* **2005**, *1*, 1232.

(35) Shiota, Y.; Suzuki, K.; Yoshizawa, K. *Organometallics* **2006**, *25*, 3118.

(36) Barone, G.; Casella, G.; Giuffrida, S.; Duca, D. *J. Phys. Chem. C* **2007**, *111*, 13033.

(37) Nash, M. J.; Shough, A. M.; Fickel, D. W.; Doren, D. J.; Lobo, R. F. *J. Am. Chem. Soc.* **2008**, *130*, 2460.

(38) (a) Nachtigallová, D.; Nachtigall, P.; Sierka, M.; Sauer, J. *Phys. Chem. Chem. Phys.* **1999**, *1*, 2019. (b) Spuhler, P.; Holthausen, M. C.; Nachtigallová, D.; Nachtigall, P.; Sauer, J. *Chem. Eur. J.* **2002**, *8*, 2099. (c) Davidová, M.; Nachtigallová, D.; Nachtigall, P.; Sauer, J. *J. Phys. Chem. B* **2004**, *108*, 13674. (d) Bludský, O.; Silhan, M.; Nachtigall, P.; Bucko, T.; Benco, L.; Hafner, J. *J. Phys. Chem. B* **2005**, *109*, 9631. (e) Bulánek, R.; Drobná, H.; Nachtigall, P.; Rubeš, M.; Bludský, O. *Phys. Chem. Chem. Phys.* **2006**, *8*, 5535.

(39) Kachurovskaya, N. A.; Zhidomirov, G. M.; van Santen, R. A. *J. Phys. Chem. B* **2004**, *108*, 5944.

(40) (a) Yumura, T.; Kertesz, M.; Iijima, S. *J. Phys. Chem. B* **2007**, *111*, 1099. (b) Yumura, T.; Kertesz, M. *Chem. Mater.* **2007**, *19*, 1028. (c) Yumura, T.; Kertesz, M.; Iijima, S. *Chem. Phys. Lett.* **2007**, *444*, 155.

(41) Frisch, M. J.; et al. *Gaussian 03*; Gaussian, Inc.: Pittsburgh, PA, 2003.

(42) (a) Becke, A. D. *Phys. Rev. A* **1988**, *38*, 3098. (b) Becke, A. D. *J. Chem. Phys.* **1993**, *98*, 5648. (c) Stephens, P. J.; Devlin, F. J.; Chabalowski, C. F.; Frisch, M. J. *J. Phys. Chem.* **1994**, *98*, 11623.

(43) Lee, C.; Yang, W.; Parr, R. G. *Phys. Rev. B* **1988**, *37*, 785.

(44) Vosko, S. H.; Wilk, L.; Nusair, M. *Can. J. Phys* **1980**, *58*, 1200.

(45) The ZSM-5 structure was taken from the Cerius 2 database; Accerys Software, Inc.: San Diego, CA.

(46) (a) Binkley, J. S.; Pople, J. A.; Hehre, W. J. *J. Am. Chem. Soc.* **1980**, *102*, 939. (b) Gordon, M. S.; Binkley, J. S.; Pople, J. A.; Pietro, W. J.; Hehre, W. J. *J. Am. Chem. Soc.* **1982**, *104*, 2797. (c) Pietro, W. J.; Francl, M. M.; Gordon, M. S.; Hehre, W. J.; Defrees, D. J.; Pople, J. A.; Binkley, J. S. *J. Am. Chem. Soc.* **1982**, *104*, 5039. (d) Dobbs, K. D.; Hehre, W. J. *J. Comput. Chem.* **1986**, *7*, 359. (e) Dobbs, K. D.; Hehre, W. J. *J. Comput. Chem.* **1987**, *8*, 861. (f) Dobbs, K. D.; Hehre, W. J. *J. Comput. Chem.* **1987**, *8*, 880.

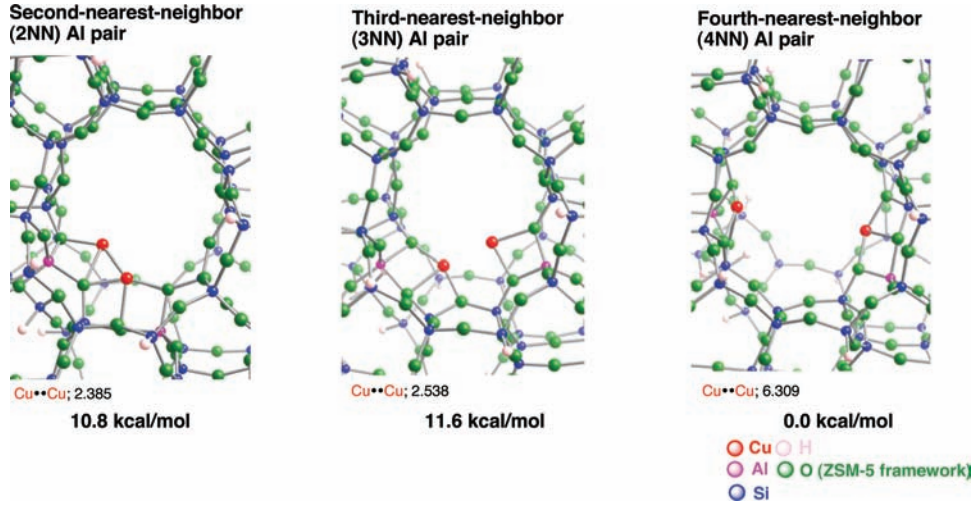

Figure 2. Local structures of three optimized Cu−ZSM-5 structures where the ZSM-5 framework was modeled as an $Al_2Si_{90}O_{151}H_{66}$ cluster. The three types of optimized structures can be distinguished by the positions of the double Si → Al substitution: the two substituted Al atoms are in second-nearest-neighbor (**2NN**), third-nearest-neighbor (**3NN**), and fourth-nearest-neighbor (**4NN**) positions in a 10-membered ring. The relative energies are given in kcal/mol. The bond lengths are in angstroms. The complete optimized geometries are given in Supporting Information Figure S1.

Chart 1

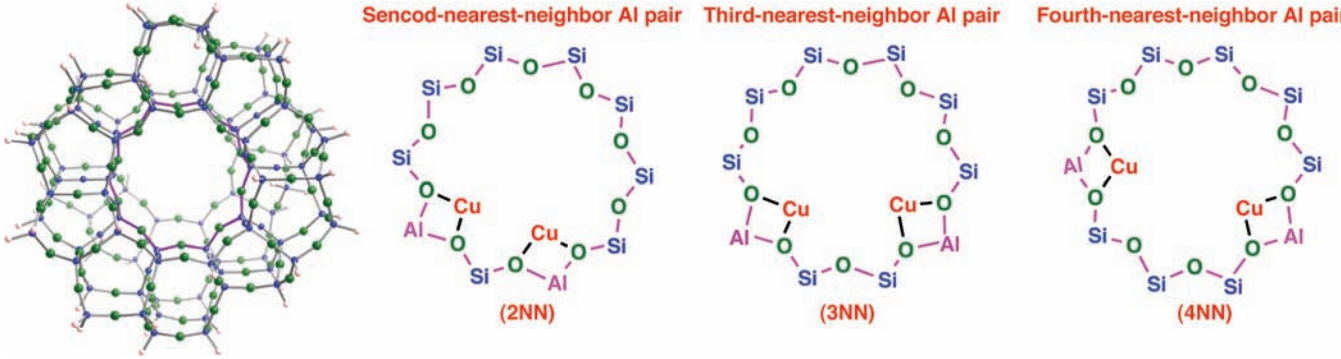

With the use of the ZSM-5 $Si_{92}O_{151}H_{66}$ cluster, we constructed Cu−ZSM-5 models in which two Cu cations are located in the vicinity of two Al atoms substituted for two Si atoms within the purple 10-MR. The purple 10-MR corresponds to its cavity at an intersection of a straight and a sinusoidal channel. Previous DFT calculations have indicated that there is no pronounced preference for substituting an Al atom for a Si atom at a particular tetrahedral site of the ZSM-5 structure.[38a] In light of the theoretical findings and Loewenstein's rule, we consider various locations for the double Si → Al substitution within the 10-MR of ZSM-5 in Chart 1, although there are many other possibilities for the substitution. As can be seen in Chart 1, the **2NN**, **3NN**, and **4NN** configurations contain the Al pairs in the second-, third-, and fourth-nearest-neighbor positions, respectively, with respect to tetrahedral sites contained in the 10-MR. Depending on the positions of the double Si → Al substitutions, the inner spaces available for the reaction vary in size. Chart 1 shows that their sizes decline in the order **4NN** > **3NN** > **2NN**, because the **4NN** (**2NN**) configuration has the widest (narrowest) separation of the Al pair, whose neighboring oxygen atoms bind coordinately to the Cu cations.

To fully optimize the geometries of the dioxygen intermediates in the Cu−ZSM-5 models, and because of the limitations of our computational resources, we used the 6-311G* basis set[47] for the Cu cations, the 6-31G* basis set[48,49] for the adsorbing dioxygen and the four O atoms that are bound to the two substituted Al atoms and simultaneously coordinated by the Cu atoms, and the 3-21G basis set[46] for the Al, Si, H, and the other O atoms in the zeolite framework. To the best of our knowledge, the magnetic properties of the dioxygen intermediates formed after the reaction between dioxygen and Cu−ZSM-5 have not been reported experimentally, so we used the closed-shell singlet spin state to obtain their local minimum. Within the B3LYP optimizations, the separation between the two Cu atoms in Cu−ZSM-5 (Figure 2) decreases in the order **4NN** (6.309 Å) > **3NN** (2.538 Å) > **2NN** (2.385 Å), as expected.[50] In the optimized Cu−ZSM-5 structures, each Cu cation coordinates to two or three oxygen atoms of the ZSM-5 framework. The Cu−O separations range from 1.90 to 2.57 Å, which is in good agreement with those obtained from EXAFS[14] and XRD[23] analyses (1.98−2.56 Å). In addition, the Cu coordination environments in the optimized structures, as well as their Cu−O separations, are consistent with previous DFT results.[31,38c] Since this consistency indicates the reliability of our choices in the present calculations, the three configurations are sufficient to investigate the ZSM-5 confinement effects.

(47) (a) Wachters, A. J. H. *J. Chem. Phys.* **1970**, *52*, 1033. (b) Hay, R. J. *J. Chem. Phys.* **1977**, *66*, 4377.

(48) (a) Hehre, W. J.; Ditchfield, R.; Pople, J. A. *J. Chem. Phys.* **1972**, *56*, 2257. (b) Francl, M. M.; Pietro, W. J.; Hehre, W. J.; Binkley, J. S.; Gordon, M. S. *J. Chem. Phys.* **1982**, *77*, 3654.

(49) Hariharan, P. C.; Pople, J. A. *Theor. Chim. Acta* **1973**, *28*, 213.

(50) The Cu−ZSM-5 structure in the **4NN** configuration is 10.8 and 11.6 kcal/mol more stable relative to those in the **2NN** and **3NN** configurations, respectively.

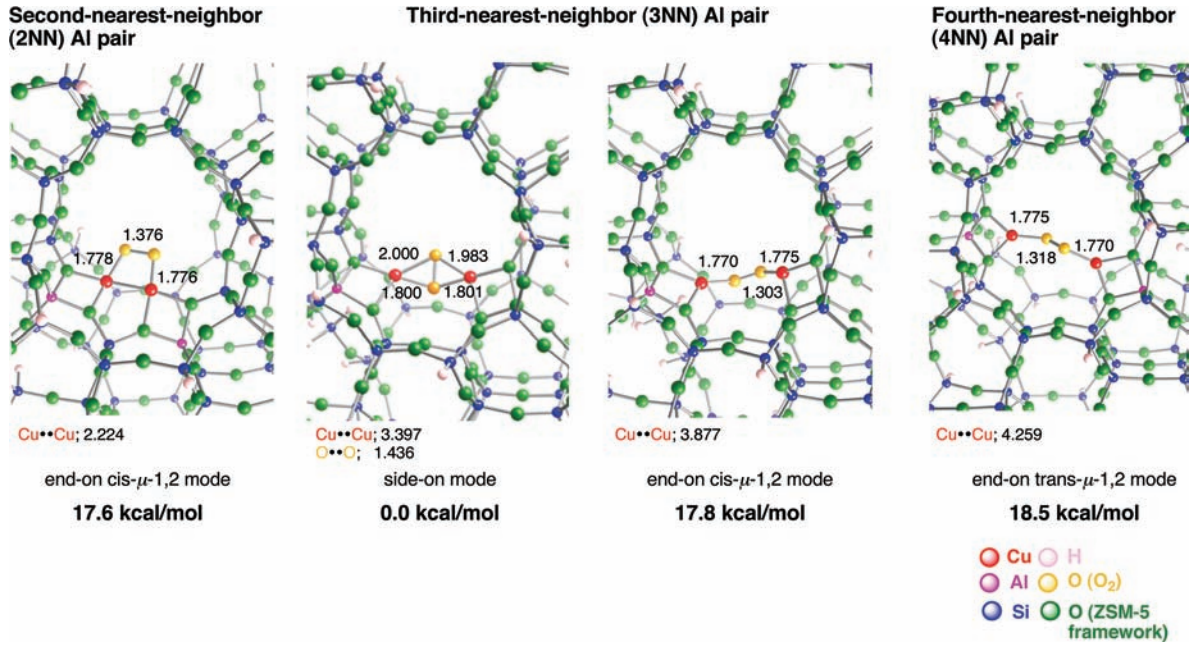

Figure 3. Local structures of four optimized $O_2\cdots Cu_2$ complexes where dioxygen binds into the two Cu cations enclosed in $Al_2Si_{90}O_{151}H_{66}$ clusters. The four types of optimized structures can be distinguished by the positions of the double Si → Al substitution: the two substituted Al atoms are in second-nearest-neighbor (**2NN**), third-nearest-neighbor (**3NN**), and fourth-nearest-neighbor (**4NN**) positions in a 10-membered ring. The relative energies are given in kcal/mol. The bond lengths are in angstroms. The complete optimized geometries are given in Supporting Information Figure S1.

Results and Discussion

Energetics of $O_2\cdots Cu_2$ Complexes. We first discuss the properties of $O_2\cdots Cu_2$ complexes where dioxygen binds to the Cu cations enclosed in the 10-MR of the ZSM-5 model. Previously, Goodman and co-workers investigated the potential energy of an $O_2\cdots Cu_2$ complex as a function of its Cu••Cu separation in a smaller ZSM-5 model and found that the Cu••Cu separation is responsible for determining their properties. According to previous DFT studies, dioxygen coordinates in an end-on cis-μ-1,2 fashion into the Cu cations, which are a distance of ∼2.5 Å apart, whereas a side-on peroxo complex has a Cu••Cu separation of ∼3.5 Å. On the other hand, there exists an end-on peroxo complex with a trans-μ-1,2 bridging mode with a Cu••Cu separation greater than 4.0 Å. On the basis of their findings, we tried to obtain local minima of $O_2\cdots Cu_2$ complexes using the more realistic ZSM-5 model in Chart 1. Since the Cu••Cu separation in the larger ZSM-5 model varies from 2.4 to 6.3 Å, depending on the locations of the Al pairs substituted in the 10-MR, we can gain direct information about the relationship between the properties of $O_2\cdots Cu_2$ complexes and the positions of the Al substitutions.

As a result of the B3LYP optimizations, we obtained one dioxygen bridging mode into the dicopper site in the **2NN** and **4NN** configurations and two modes in the **3NN** configuration. The local and complete structures of the four optimized complexes are given in Figure 3 and Figure S1 (Supporting Information), respectively. The relative stability of the four $O_2\cdots Cu_2$ complexes is shown in Figure 3. In the **2NN** (**4NN**) configuration, dioxygen binds to the Cu cations in an end-on cis-μ-1,2 (trans-μ-1,2) fashion, whereas the **3NN** configuration has a side-on peroxo-bridged dicopper complex as well as an end-on complex with a cis-μ-1,2 mode.[51] In the **3NN** configuration, the side-on form is 17.8 kcal/mol more stable relative to the end-on form. The preference for the side-on bridging mode appears to be quite

(51) We cannot obtain optimized side-on peroxo complexes in the **2NN** and **4NN** configurations. Instead, we obtained the optimized end-on peroxo complex with a trans-μ-1,2 mode in the **4NN** configuration. After the dioxygen binding, the **4NN** Cu−ZSM-5 structure is deformed, and the two Cu cations are significantly pushed off the ZSM-5 framework to a separation of 4.3 Å. As shown in Table 1, the geometrical deformation of Cu−ZSM-5 requires 41.1 kcal/mol, which is significant relative to those in the **2NN** and **3NN** configurations. To obtain an optimal Cu••Cu separation for the dioxygen binding in a side-on fashion (∼3.5 Å) (ref 22), a further geometrical deformation is necessary. Consequently, the Cu−ZSM-5 structure is expected to be additionally destabilized. Such destabilization can prevent dioxygen from binding in a side-on fashion to the dicopper active site. To justify the above discussion, we performed partial optimizations of an O_2••Cu_2 structure in the **4NN** configuration where the dioxygen O−O bond is fixed at 1.45 Å (a typical peroxo bond in a side-on fashion). The partially optimized geometry with the O−O bond at 1.45 Å still has an end-on form and is 5.5 kcal/mol more unstable relative to the fully optimized end-on peroxo complex. It seems that a peroxo species with an O−O bond of ∼1.45 Å cannot bind in a side-on fashion to the two Cu cations of the **4NN** configuration. In contrast, the **2NN** configuration does not have a space where the Cu cations are allowed to migrate from their original position of its Cu−ZSM-5. Please note that the optimized end-on peroxo complex has a Cu••Cu separation of 2.224 Å (Figure 3), which is shorter than that in the O_2-free Cu−ZSM-5 (2.385 Å). It is difficult for dioxygen to bind to the dicopper active site in a side-on fashion, while keeping its O−O bond of ∼1.4 Å. Actually, we used a side-on peroxo complex as an initial geometry in the **2NN** configuration. However, we could not obtain the side-on peroxo form. During the B3LYP optimization, the dioxygen O−O bond breaks, and eventually the initial geometry converted into a bis(μ-oxo) dicopper species. The initial geometry with a side-on bridging mode is 62.7 and 52.2 kcal/mol more unstable in energy relative to the optimized end-on peroxo and bis(μ-oxo) dicopper complexes in the **2NN** configuration, respectively. Moreover, we can see in Figure 5 that the optimized Cu••Cu separation in the bis(μ-oxo) dicopper complex in the **2NN** configuration (2.787 Å) is significantly shorter than the optimal Cu••Cu separation for a side-on peroxo complex as obtained in ref 22. This result also suggests that the **2NN** configuration does not allow dioxygen to bind to the dicopper active site in a side-on fashion.

Table 1. Energetics of the Optimized $O_2\cdots Cu_2$ Complexes in the ZSM-5 Model

	O_2 bridging mode	E_{BE}[a]	ΔE[b]
2NN configuration[c]	end-on cis-μ-1,2 mode	−45.4	19.9
3NN configuration[c]	end-on cis-μ-1,2 mode	−46.2	22.0
3NN configuration[c]	side-on mode	−64.0	27.9
4NN configuration[c]	end-on trans-μ-1,2 mode	−34.0	41.1

[a] $E_{BE} = E(O_2\cdots Cu{-}ZSM\text{-}5) - E(Cu{-}ZSM\text{-}5) - E(O_2)$. [b] $\Delta E = E$(deformed Cu−ZSM-5) − E(Cu−ZSM-5). [c] The **2NN**, **3NN**, and **4NN** configurations have the Al pairs in second-, third-, and fourth-nearest-neighbor positions, respectively, in a 10-membered ring in the ZSM-5 model.

unique, compared with the case of diiron peroxo complexes, where the end-on bridging mode is favored.[21c,52,53] The energy differences between the side-on and end-on complexes (17.8−18.5 kcal/mol in Figure 3) are comparable to those obtained in the smaller $Cu{-}Al_2(OH)_8$ model (∼12 kcal/mol),[22] suggesting that the zeolite confinement does not have a significant influence on the $O_2\cdots Cu_2$ complexes.

In contrast to the findings described in ref 22, the new large-scale DFT calculations indicate that the positions of the Al substitutions strongly affect the modes of dioxygen bridging into a dicopper active site inside the 10-MR; from the viewpoint of energetics, the end-on forms are feasible in the **2NN** and **4NN** configurations, whereas the side-on form is preferred in the **3NN** configuration. Table 1 shows the binding energies of the $O_2\cdots Cu_2$ complexes calculated by $E_{BE} = E(O_2\cdots Cu{-}ZSM\text{-}5) - E(Cu{-}ZSM\text{-}5) - E(O_2)$. Here, $E(O_2\cdots Cu{-}ZSM\text{-}5)$ and $E(Cu{-}ZSM\text{-}5)$ represent the total energies of an $O_2\cdots Cu$ complex (Figure 3) and an O_2-free Cu−ZSM-5 (Figure 2), respectively. A negative E_{BE} value indicates that dioxygen is preferentially bound to a dicopper active site of ZSM-5. Table 1 shows that all dioxygen additions are exothermic. Their calculated binding energies vary, depending on the dioxygen bridging modes as well as the Al positions. The stabilization energy in the side-on peroxo complex is 64.0 kcal/mol, which is larger than those obtained in the end-on peroxo complexes (34.0−46.2 kcal/mol).[54]

Additionally, the large-scale DFT calculations reveal that the coordination environments of the Cu cations are changed by the formation of the new Cu−O bonds (1.77−2.00 Å). As shown in Figures 2 and 3, both Cu cations migrate from their original positions in an O_2-free Cu−ZSM-5, and their separation then becomes suitable for the binding of dioxygen in an end-on or a side-on fashion. We see different Cu··Cu separations depending on the dioxygen bridging modes; the optimized Cu··Cu separation in the side-on peroxo complex is 3.397 Å, whereas that in the end-on peroxo complex with a cis-μ-1,2 (trans-μ-1,2) fashion is 2.224 (4.259) Å. The optimal Cu··Cu separations for a dioxygen bridging mode obtained from the large-scale DFT calculations are similar to those reported by Goodman and co-workers.[22] The Cu migration destabilizes the Cu−ZSM-5 structure itself, as can be estimated by the energy difference between an O_2-free Cu−ZSM-5 and a Cu−ZSM-5 deformed by the dioxygen binding, $\Delta E = E$(deformed Cu−ZSM-5) − E(Cu−ZSM-5). Here, E(deformed Cu−ZSM-5) is the single-point energy of a deformed Cu−ZSM-5 taken from an optimized $O_2\cdots Cu{-}ZSM\text{-}5$ structure. A positive ΔE value indicates that the Cu−ZSM-5 is destabilized by the Cu migration. As expected, we obtained positive ΔE values in all the configurations in Table 1. Moreover, the destabilization strongly depends on the positions of the Al substitutions. In fact, the ΔE value decreases in the order **4NN** > **3NN** > **2NN**. The DFT findings indicate that the positions of the Al substitutions in a 10-MR govern whether the Cu cations can migrate easily to fit dioxygen binding in a given fashion. Thus, the geometric changes in the Cu−ZSM-5 are among the key factors in determining the preferable dioxygen bridging modes within the 10-MR,[51] although the destabilization is compensated for by strong attractive interactions between dioxygen and a Cu−ZSM-5.

In the present study, we confined our discussion to the $O_2\cdots Cu_2$ complexes in the closed-shell singlet state, because, until now, antiferromagnetic couplings between the Cu(II) cations have not been reported experimentally in the ZSM-5 system. On the other hand, analogous peroxo-bridged dicopper(II) complexes with nitrogen-based ligands have a singlet biradical ground state through antiparallel couplings of the spins on the opposite Cu(II) centers.[55] Thus, it is interesting to investigate whether the open-shell (OS) singlet biradical state of an $O_2\cdots Cu$ complex in ZSM-5 can compete in energy with its closed-shell (CS) singlet state. To describe the singlet biradical systems, we used the unrestricted broken-symmetry (BS) approach. However, the BS approach is time-consuming, in particular for large-scale DFT calculations. Thus, we performed single-point energy calculations with the four optimized $O_2\cdots Cu_2$ complexes (Figure 3) using the BS approach to obtain the OS singlet state.[56,57] As shown in Table S1 (Supporting Information), in the B3LYP method the $O_2\cdots Cu_2$ complexes in the OS singlet state[58] are 2.3−9.8 kcal/mol more stable relative to those in the CS singlet state. The energy difference increases as the Cu··Cu separation increases. However, the B3LYP method often overstabilizes biradical singlet $O_2\cdots Cu_2$ systems.[56,57] The erroneous overstabilization in the BS B3LYP method is associated with the inadequacy of a single Kohn−Sham (KS) determinant as a description of the biradical systems. Also, inclusion of

(52) (a) Yoshizawa, K.; Hoffmann, R. *Inorg. Chem.* **1996**, *35*, 2409. (b) Yoshizawa, K.; Yokomichi, Y.; Shiota, Y.; Ohta, T.; Yamabe, T. *Chem. Lett.* **1997**, 587. (c) Yoshizawa, K.; Yumura, T. *Chem. Eur. J.* **2003**, *9*, 2347. (d) Yumura, T.; Yoshizawa, K. *Bull. Chem. Soc. Jpn.* **2004**, *77*, 1305.
(53) Han, W.-G.; Noodleman, L. *Inorg. Chem.* **2008**, *47*, 2975.
(54) In the end-on peroxo complexes, the differences in the calculated binding energies are related to the stability of the O_2-free Cu−ZSM-5 structures. See ref 50.
(55) Karlin, K. D.; Tyklár, Z.; Farooq, A.; Jacobson, R. R.; Sinn, E.; Lee, D. W.; Bradshaw, J. E.; Wilson, L. J. *Inorg. Chim. Acta* **1991**, *182*, 1.
(56) Rode, M. F.; Werner, H.-J. *Theor, Chem. Acc.* **2005**, *114*, 309.
(57) Cramer, C. J.; Wloch, M.; Piecuch, P.; Puzzarini, C.; Gagliardi, L. *J. Phys. Chem. A* **2006**, *110*, 1991.
(58) The broken-symmetry (BS) state ($E_{\langle Sz\rangle=0}$) is not a pure spin state described by a single determinant but rather a weighted average of pure spin states. To eliminate spin contamination from the triplet spin state ($E_{\langle Sz\rangle=1}$) in the BS-SCF solution, the open-shell (OS) singlet state energy (E_{OS}) was defined (ref 57) as $(2E_{\langle Sz\rangle=0} - \langle S^2\rangle E_{\langle Sz\rangle=1})/(2 - \langle S^2\rangle)$, where the triplet spin state energy was obtained by single-point energy calculations with the optimized geometry (Figure 2) and $\langle S^2\rangle$ is the expectation value of the total-spin operator in the BS state. We used E_{OS} values to obtain energy differences between the OS and closed-shell (CS) singlet spin states in Table S1 (Supporting Information).

the Hartree−Fock exchange in hybrid functionals seems to result in overstabilizing of singlet biradical dicopper(II) systems.[57] Instead, we used a pure DFT method with the PW91 functional to evaluate the CS−OS energy difference, according to ref 53. In the PW91 method, the CS−OS energy differences, which range from 0.8 to 3.5 kcal/mol,[59] are significantly smaller than those obtained by the B3LYP calculations. Thus, we found that the CS−OS energy differences are sensitive to the DFT functionals used, although from an energetics viewpoint the peroxo-bridged dicopper complexes may have antiferromagnetically coupled Cu(II) sites, as shown in Table S1 (Supporting Information). Up to now, it has been uncertain which functionals can correctly describe the geometrical features as well as the electronic properties, especially the magnetic couplings, of these complexes. Despite the uncertainty, these preliminary theoretical findings should stimulate not only experimental efforts to observe antiferromagnetic couplings between the Cu(II) cations in ZSM-5 but also theoretical developments to precisely calculate the biradical state of such large systems.

O−O Bond Activation in the $O_2\cdots Cu_2$ Complexes. Since the magnetic couplings between the two Cu cations have remained experimentally unknown, we return our attention to the dioxygen activation in the $O_2\cdots Cu_2$ complexes in the CS singlet state. The dioxygen O−O bond lengths vary significantly between the various bridging modes, as shown in Figure 3. The O−O bond in the side-on peroxo complex, whose length was computed to be 1.436 Å, is significantly activated relative to the free dioxygen case. The computed value is also substantially larger than those in the end-on peroxo complexes (1.303−1.376 Å). In the end-on peroxo complexes, the Cu··Cu separation, which depends on the positions of the Al substitutions, determines their dioxygen O−O bond length.[60,61] In the **2NN** configuration, the end-on complex has an O−O bond of 1.379 Å, whereas slightly shorter peroxo O−O bonds (∼1.31 Å)[62] are found in the **3NN** and **4NN** configurations. These findings suggest that vibrational analyses of O−O stretching modes provide a clue not only to the dioxygen bridging modes into the dicopper active site[63] but also to the locations of the substituted Al atoms within a 10-MR.

In order to clarify why the dioxygen bridging modes and the Cu··Cu separations are important to the dioxygen activation, useful information can be derived from their frontier orbitals, whose amplitudes are localized mainly in the $O_2\cdots Cu_2$ cores, as shown in Figure 4. Here, we pay attention to the energetically preferable peroxo forms in the three configurations. Figure 4 shows that the three peroxo forms exhibit quite different electronic properties. In the frontier orbital region of the end-on form in the **2NN** configuration, only one occupied orbital (the highest occupied molecular orbital (HOMO)) appears, and it lies ∼1.2 eV above the next HOMO (HOMO−1). In the HOMO, which should make a key contribution to the $O_2\cdots Cu_2$ structure, there is the antibonding π orbital with respect to the dioxygen O−O bond. The out-of-phase interactions between the two O atoms are an important factor in lengthening their bond length.

Unlike the **2NN** case, two occupied orbitals lie in the frontier orbital regions of the **3NN** and **4NN** cases. In the **3NN** configuration, where dioxygen binds to the two Cu cations in a side-on fashion, the HOMO and HOMO−1 consist of antibonding couplings between the two O atoms. This is one of the main reasons that the side-on form has an O−O bond longer than those in the end-on forms. In contrast, the end-on form in the **4NN** configuration has in-phase and out-of-phase interactions between the two O atoms of dioxygen in the HOMO and the HOMO−1, respectively. The repulsive forces between the two O atoms, derived from the antibonding characters in the HOMO−1, are similar to the **2NN** case. However, the repulsive couplings in the **4NN** case are diminished by attractive interactions due to the bonding characters in the HOMO. The cancelations account for the shorter O−O bond lengths in the **4NN** case than in the **2NN** case. Judging from the Cu··Cu separations in the end-on forms, the striking differences in the electronic properties between the **2NN** and **4NN** cases are due to interactions between the two Cu cations.[60,61] Thus, the orbital interaction analyses (Figure 4) may illuminate the fact that the Al substitution positions dominate the activation of the dioxygen O−O bond in the end-on forms through the Cu··Cu interactions.

Bis(μ-oxo)dicopper Complexes. Next, we investigate how the ZSM-5 cavity affects the properties of bis(μ-oxo)dicopper complexes generated by cleaving the dioxygen O−O bond in the $O_2\cdots Cu_2$ complexes. The three optimized structures of bis(μ-oxo)dicopper complexes are shown, with their local structures surrounding the active sites, in Figure 5. The two oxo ligands are separated by ∼2.1 Å.[64] We can also see similarities in the bond distances in diamond Cu_2O_2 cores of the three bis(μ-oxo)dicopper complexes, irrespective of the positions of the Al atom substitutions; the optimized Cu−O bonds range from 1.74 to 1.83 Å, and the Cu··Cu separations fall in the range of 2.76−2.87 Å, as shown in Figure 5.

Despite their similar Cu−O bondings, the diamond Cu_2O_2 cores have quite different structural features in terms of their

(59) We also calculated the CS−OS energy difference ($E_{CS-OS} = E_{CS} - E_{OS}$) using another pure DFT method using the BLYP functional, because the BLYP method can give a reliable unrestricted solution and then can reproduce experimental data (ref 57). In the BLYP method, the calculated CS−OS energy differences also have small values of up to 3.5 kcal/mol. The BLYP results are essentially consistent with the PW91 results.

(60) Thorn, D. T.; Hoffmann, R. *Inorg. Chem.* **1978**, *17*, 126.

(61) Mehrotra, P. K.; Hoffmann, R. *Inorg. Chem.* **1977**, *17*, 2187.

(62) To justify our DFT results that the end-on peroxo complexes in the **3NN** and **4NN** configurations have the short peroxo bonds in Figure 3, we replaced the 6-31G* basis set for dioxygen with the 6-31+G* basis set and then reoptimized their $O_2\cdots Cu_2$ complexes. As a result of the reoptimization using the diffuse function for dioxygen, the optimized O−O bond lengths in the **3NN** and **4NN** configurations are 1.319 and 1.313 Å, respectively. These values are fully consistent with those obtained using the 6-31G* basis set for the dioxygen (Figure 3). The short peroxo O−O bonds are characteristic of the end-on peroxo complexes relative to the side-on peroxo complex, because of the different electronic properties in the frontier orbital regions between the two forms in Figure 4. Also see ref 12.

(63) Cramer, C. J.; Tolman, W. B.; Theopold, K. H.; Rheingold, A. L. *Proc. Natl. Acad. Sci. U.S.A.* **2003**, *100*, 3635.

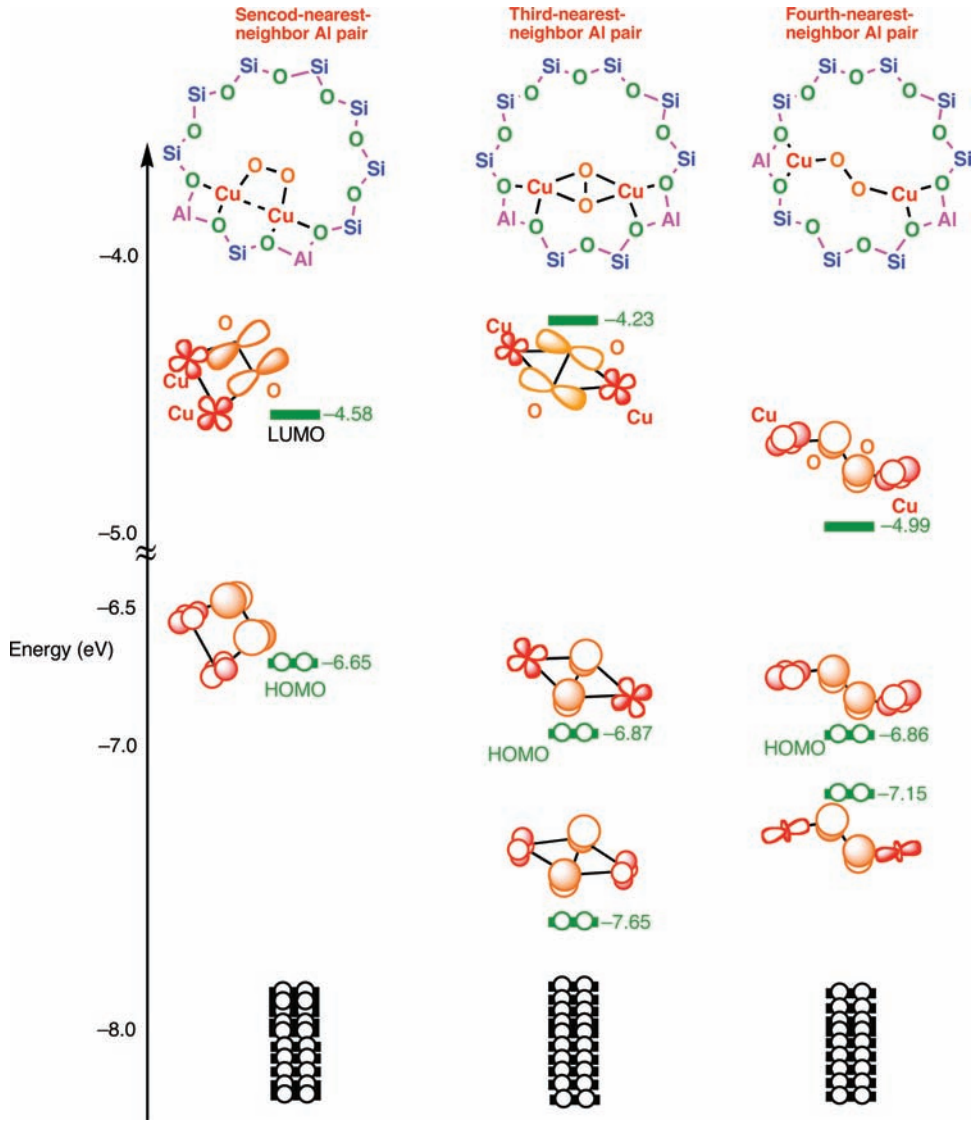

Figure 4. Frontier orbitals of the three types of optimized $O_2\cdots Cu_2$ complexes inside the $Al_2Si_{90}O_{151}H_{66}$ clusters, depending on the positions of the double Si → Al substitution (second-nearest-neighbor (**2NN**), third-nearest-neighbor (**3NN**), and fourth-nearest-neighbor (**4NN**) Al pairs). Energy levels of the orbitals, based on the couplings between d(Cu) and p(O) orbitals, are given in eV. Their orbital amplitudes are also shown.

planarity. The **4NN** configuration has a nearly planar Cu_2O_2 structure, whose dihedral angle is 0.4°, whereas the **2NN** and **3NN** configurations have Cu_2O_2 structures distorted from a planar structure (the dihedral angles in the **2NN** and **3NN** cases are 25.4° and 25.7°, respectively). These structural differences in the bis(μ-oxo)dicopper complexes should reflect whether a configuration has enough room to accommodate a planar diamond Cu_2O_2 core; the **4NN** configuration, where the substituted Al atoms are nearly diametrically opposed, can contain a planar structure in the 10-MR, whereas the **2NN** and **3NN** configurations cannot. Accordingly, these restrictions make the diamond cores adopt butterfly structures, as shown in Figure 5.

Along with the structural differences of the diamond Cu_2O_2 cores in the three configurations, the coordination environments of the two Cu(III) cations vary significantly. As shown in Figure 5, the **4NN** (**2NN**) configuration possesses Cu(III) cations coordinating four oxygen atoms in a nearly square planar (a tetrahedral) manner. The differences in the Cu coordination should govern their stability, in light of the relationships between the coordination environments of transition-metal atoms and their stability.[65] Chart 2 shows the d splittings of square planar and tetrahedral Cu(III)L_4 complexes, where L represents a ligand.[65] In Chart 2, a tetrahedral Cu(III)L_4 complex has two low-lying e orbitals

(64) To investigate whether the bis(μ-oxo) dicopper species in the singlet spin state is energetically stable relative to those in the triplet and quintet spin states, we performed single-point energy calculations with the optimized structures (Figure 5). In the **2NN** configuration, the singlet spin state lies 5.0 and 13.5 kcal/mol below the triplet and quintet spin states, respectively. The **3NN** (**4NN**) configuration has the singlet spin state being 14.1 (16.8) and 14.8 (28.2) kcal/mol more stable than the triplet and quintet spin states, respectively. According to the DFT calculations, the bis(μ-oxo) dicopper species have the singlet ground state, which is consistent with the lack of an EPR signal for the species in ref 15. Note that the energy difference between the single and quintet spin states increases in the order **2NN** < **3NN** < **4NN**. This order should reflect their electronic properties in the frontier orbital region, especially the HOMO−LUMO gap. See Chart 2 and Figure S2 (Supporting Information).

(65) Albright, T. A.; Burdet, J. K.; Whangbo, M.-H. *Orbital Interactions in Chemistry*; John Wiley & Sons, Inc.: New York, 1985.

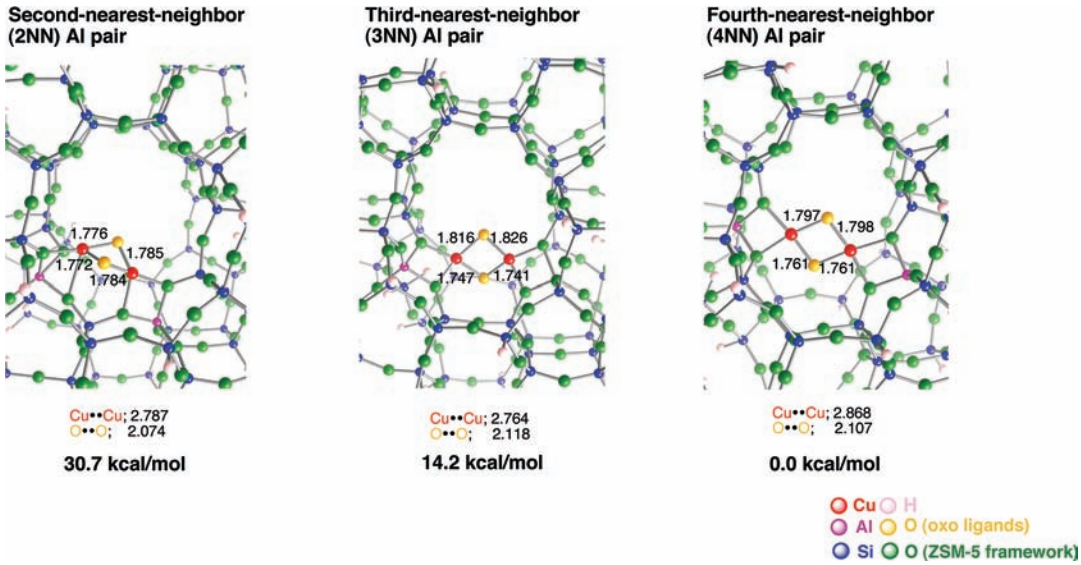

Figure 5. Local structures of three optimized bis(μ-oxo)dicopper complexes where two oxo ligands coordinate the two Cu cations inside $Al_2Si_{90}O_{151}H_{66}$ clusters. The three types of optimized structures can be distinguished by the positions of the double Si → Al substitution: the two substituted Al atoms are in second-nearest-neighbor (**2NN**), third-nearest-neighbor (**3NN**), and fourth-nearest-neighbor (**4NN**) positions in a 10-membered ring. The relative energies are given in kcal/mol. The bond lengths are in angstroms. The complete optimized geometries are given in Supporting Information Figure S1.

Chart 2

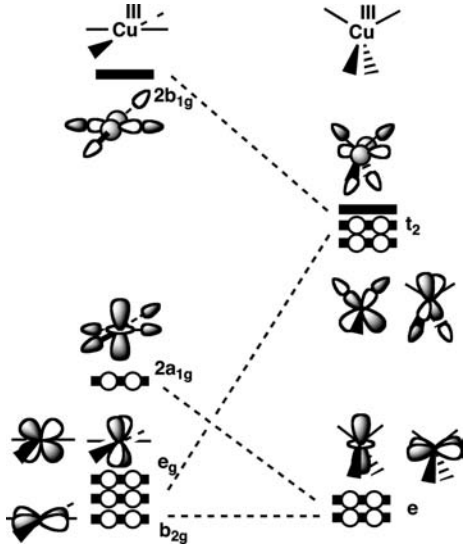

and three high-lying t_2 orbitals. In contrast with a tetrahedral Cu(III)L_4 complex, one of the t_2 orbitals is destabilized in a square planar Cu(III)L_4 complex, whereas the other two t_2 orbitals are stabilized. At the same time, the degeneracy of the e orbitals is lifted in a square planar Cu(III)L_4 complex, where one is destabilized to generate the $2a_{1g}$ orbital, and the energy of the other remains unchanged. We can justify the qualitative interpretations of their frontier orbitals with the DFT calculations in Figure S2 (Supporting Information), which shows the orbital energies in the frontier orbital regions. For example, the DFT calculations show that the energies of the lowest unoccupied molecular orbitals (LUMOs) in the bis(μ-oxo) dicopper species are significantly shifted upward as the dihedral angle of the Cu_2O_2 structure decreases. From the viewpoint of d splittings in Chart 2, a Cu(III)L_4 complex preferentially adopts a planar structure instead of a tetrahedral structure as a result of the destabilization of the highest occupied MO (t_2) on the tetrahedral side relative to the HOMO ($2a_{1g}$) on the planar side.

This simple argument can be applied to their stability, as obtained by DFT calculations. Figure 5 shows that the **4NN** configuration, where both Cu cations have square planar coordination, is the most stable energetically, as it is 14.2 and 30.7 kcal/mol more stable relative to those in the **3NN** and **2NN** configurations, respectively. These energy differences are more pronounced than in the $O_2\cdots Cu_2$ cases, which can be ascribed to the different sizes of the enclosed Cu_2O_2 structures between the two intermediates. In the $O_2\cdots Cu_2$ complexes, the binding of dioxygen into the two Cu cations requires one side of the line connecting the two Cu cations, whereas the bis(μ-oxo)dicopper species require both sides to form the four Cu−O bonds. In other words, cleaving the dioxygen O−O bond differentiates the bis(μ-oxo) dicopper species from the $O_2\cdots Cu_2$ complexes in terms of the sizes of Cu_2O_2 cores. Since the three bis(μ-oxo)dicopper complexes have strikingly different Cu coordination environments, due to the confinement of a diamond Cu_2O_2 guest inside a ZSM-5 host, the bis(μ-oxo)dicopper complexes are more susceptible than the $O_2\cdots Cu_2$ complexes to special constraints from the ZSM-5.

Dioxygen Activation Mediated by Dicopper Cations Enclosed inside ZSM-5. Finally, we examine the energetics of the reaction intermediates along the dioxygen activation pathway in order to investigate whether the intermediates can be formed within the zeolite. Table 2 tabulates the relative energies of the intermediates with respect to the dissociation limit toward dioxygen and Cu−ZSM-5. The initial step of the dioxygen activation, in which dioxygen binds to the enclosed Cu cations, is energetically preferable irrespective of the locations of the two Al atoms that substitute for the two Si atoms. The stabilization due to the dioxygen binding can facilitate subsequent reaction steps, at least the conversion of an $O_2\cdots Cu_2$ complex to a bis(μ-

Table 2. Energies (kcal/mol) of Dioxygen Intermediates Formed during the Dioxygen Activation by Cu−ZSM-5, Relative to the Dissociation Limit toward Cu−ZSM-5 ($Cu-Al_2Si_{90}O_{151}H_{66}$) and Dioxygen

	$O_2\cdots Cu_2$ complex	bis(μ-oxo)dicopper complex
2NN configuration[a]	−45.4	−34.9
3NN configuration[a]	−64.0[b]	−52.3
4NN configuration[a]	−34.0	−54.9

[a] The **2NN**, **3NN**, and **4NN** configurations have the Al pairs in second-, third-, and fourth-nearest-neighbor positions, respectively, in a 10-membered ring in the ZSM-5 model. [b] The relative energy of the side-on peroxo complex in the **3NN** configuration is listed.

oxo)dicopper complex. In fact, we can see in Table 2 that the bis(μ-oxo)dicopper complexes that are formed by cleaving the dioxygen O−O bond in the $O_2\cdots Cu_2$ complexes lie below the dissociation limit. Thus, the bis(μ-oxo)dicopper complexes can be easily formed inside the 10-MR of the ZSM-5, although we did not evaluate the activation energy for the cleavage of the dioxygen O−O bond in the present study.

Table 2 also shows that the ZSM-5 confinement plays a significant role in the relative stability of the dioxygen intermediates. In the **2NN** and **3NN** configurations, the $O_2\cdots Cu_2$ complexes are, respectively, 10.5 and 11.7 kcal/mol more stable relative to the bis(μ-oxo)dicopper complexes, in contrast to the **4NN** case, where the bis(μ-oxo)dicopper complex is energetically favored.[66] The destabilization of the bis(μ-oxo)dicopper complexes relative to the $O_2\cdots Cu_2$ complexes in the **2NN** and **3NN** configurations comes from the tight spatial restrictions, as mentioned above. The importance of the ZSM-5 constraint to their stability is unique in zeolite systems, as compared with synthetic Cu_2O_2 models.[67] Since the bis(μ-oxo) dicopper complexes can act as direct intermediates for methane oxidation, a restricted ZSM-5 environment should contribute to the catalytic activity of Cu−ZSM-5 by adjusting the stability of its active species. This is the first theoretical report obtained from large-scale DFT calculations that has illuminated the roles of the ZSM-5 surroundings in the catalytic activity mediated by enclosed Cu_2O_2 cores, although Bhan and Iglesia recently suggested an experimental link between reactivity and local structure in acid catalysis in zeolites.[68]

Conclusions

At the level of B3LYP theory, we analyzed the properties of dioxygen intermediates generated during the activation of dioxygen by two Cu cations enclosed in a 10-MR of ZSM-5. In order to investigate how the ZSM-5 nanospaces affect their properties, three types of configurations were considered in which two Al atoms replace two Si atoms in a 10-MR: the configurations in which the Al pairs are in second-, third-, and fourth-nearest-neighbor positions with respect to their tetrahedral sites in the **2NN**, **3NN**, and **4NN** configurations, respectively. Judging from the Cu··Cu separations in the three Cu−ZSM-5 configurations, the inner spaces available for the reaction decrease in size in the order **4NN** > **3NN** > **2NN**. In the first intermediates, $O_2\cdots Cu_2$ complexes where dioxygen binds to the two Cu cations, the zeolite confinement effects are not significant because the inner spaces are large enough to form new Cu−O bonds. Instead, the positions of the substituted Al atoms in a 10-MR play a crucial role in determining the type of dioxygen bridging (an end-on or a side-on fashion). The dioxygen O−O bond is activated differently depending on the dioxygen bridging fashions, as well as the Cu··Cu separation.

In contrast, the second intermediates, bis(μ-oxo) dicopper complexes following the $O_2\cdots Cu_2$ complexes by cleaving the dioxygen O−O bond, are more subject to spatial constraints from the ZSM-5 because the contained diamond Cu_2O_2 cores need larger spaces to form four Cu−O bonds. Because of the limited inner space available in the **2NN** configuration, its diamond core has a butterfly form with a Cu tetrahedral coordination. On the contrary, the **4NN** configuration does not have such a restriction and thus possesses a diamond core where each Cu cation is coordinated by four oxygen atoms in a square planar manner. Since the tetrahedral Cu(III) coordination is not energetically preferable relative to the square planar coordination, the bis(μ-oxo)dicopper complex in the **4NN** configuration is 30.7 kcal/mol more stable relative to the **2NN** case. The DFT results show more pronounced ZSM-5 confinement effects in the bis(μ-oxo)dicopper complexes than the $O_2\cdots Cu_2$ cases. Accordingly, the spatial constraint from the ZSM-5 has a strong impact on energy profiles along the dioxygen activation by Cu−ZSM-5. These effects should be important in direct methane activation derived from the bis(μ-oxo)dicopper complexes.

Acknowledgment. This work was supported by the Japan Society for the Promotion of Science (JSPS) for T.Y.

Supporting Information Available: Complete optimized geometries of the Cu−ZSM-5 model ($Cu_2-Al_2Si_{90}O_{151}H_{66}$), the $O_2\cdots Cu_2$ complexes, and the bis(μ-oxo)dicopper complexes (Figure S1), the orbital energy diagrams in the frontier orbital region of bis(μ-oxo) dicopper complexes (Figure S2), the energy differences in the $O_2\cdots Cu_2$ complexes between the closed-shell (CS) and open-shell (OS) singlet spin states (Table S1), and full author list for ref 41. This material is available free of charge via the Internet at http://pubs.acs.org.

IC8010184

(66) We obtained the energy differences between an $O_2\cdots Cu_2$ complex and a bis(μ-oxo) complexes in the closed-shell singlet state in Table 2. Even if we consider that the $O_2\cdots Cu_2$ complexes have the singlet biradical ground state, as shown in Table S1 (Supporting Information), we can obtain the same results in terms of the relative stability; the $O_2\cdots Cu_2$ complexes are stable relative to the bis(μ-oxo) dicopper complexes in the **2NN** and **3NN** configurations, whereas the bis(μ-oxo) dicopper complex is favored in the **4NN** configuration.

(67) (a) Henson, M. J.; Vance, M. A.; Zhang, C. X.; Liang, H.-C.; Karlin, K. D.; Solomon, E. I. *J. Am. Chem. Soc.* **2003**, *125*, 5186. (b) Liang, H.-C.; Henson, M. J.; Hatcher, L. Q.; Vance, M. A.; Zhang, C. X.; Lahti, D.; Kaderli, S.; Sommer, R. D.; Rheingold, A. L.; Zuberbühler, A. D.; Solomon, E. I.; Karlin, K. D. *Inorg. Chem.* **2004**, *43*, 4115. (c) Hatcher, L. Q.; Vance, M. A.; Sarjeant, A. A. N.; Solomon, E. I.; Karlin, K. D. *Inorg. Chem.* **2006**, *45*, 3004.

(68) Bhan, A.; Iglesia, E. *Acc. Chem. Res.* **2008**, *41*, 559.